Tandem methanolysis and catalytic transfer hydrogenolysis of polyethylene terephthalate to p-xylene over Cu/ZnZrO$_x$ catalysts

Ryan Helmer,[a] Siddhesh S. Borkar,[a] Aojie Li,[b] Fatima Mahnaz,[a] Jenna Vito,[a] Michelle Bishop,[a] Ashfaq Iftakher,[a] M.M. Faruque Hasan[a,c] Srinivas Rangarajan,[b] and Manish Shetty*[a]

R. Helmer, S.S. Borkar, F. Mahnaz, J. Vito, A. Iftakher, Prof. M.M.F. Hasan, and Prof. M. Shetty

Artie McFerrin Department of Chemical Engineering, Texas A&M University

100 Spence Street, College Station, TX-77843. USA.

E-mail: manish.shetty@tamu.edu

[b] Aojie Li, and Prof. S. Rangarajan
Chemical and Biomolecular Engineering, Lehigh University

HST Building, L136 124 E. Morton Street, Bethlehem, PA 18015. USA.

[c] Prof. M.M.F. Hasan
Texas A&M Energy Institute
617 Research Parkway, College Station, TX-77843-3372.

Abstract: We demonstrate a novel approach of utilizing methanol (CH_3OH) for both the methanolysis of polyethylene terephthalate (PET) to form dimethyl terephthalate (DMT) at near-quantitative yields (~97%) and catalytic transfer hydrogenolysis (CTH) of DMT to p-xylene (PX, ~63% at 240 °C and 16 h) on a reducible $ZnZrO_x$ supported Cu catalyst (i.e., $Cu/ZnZrO_x$). Pre- and post-reaction surface and bulk characterization, along with density functional theory (DFT) computations, explicate the role of the metal-support interface of $Cu/ZnZrO_x$ in providing active sites for the activation of both CH_3OH and DMT and facilitating a lower free-energy pathway for both CH_3OH dehydrogenation and DMT hydrogenolysis, compared to Cu supported on redox-neutral SiO_2 support. DFT calculations further reveal that the rate-determining step for CTH of DMT is the cleavage of the C-O linkages in –(C=O)-OR) of DMT. Loading studies and thermodynamic calculations showed that, under reaction conditions, CH_3OH in the gas phase, rather than in the liquid phase, is critical for CTH of DMT. Interestingly, the $Cu/ZnZrO_x$ catalyst was also effective for the methanolysis and hydrogenolysis of C-C bonds (compared to C-O bonds for PET) of waste polycarbonate (PC), largely forming xylenol (~38%) and methyl isopropyl anisole (~42%) demonstrating the versatility of this approach toward valorizing a wide range of condensation polymers.

Introduction

The ubiquity of plastic waste and their descendent microplastics, from marine ecosystems to the human body,[1-3] presents a challenge for waste management but also potentially acts as a valuable carbon source for producing fuels and chemicals. Polyethylene terephthalate (PET) is the most produced polyester annually in the world[4] due to its many applications, including textiles, engineering resins, and packaging.[4] Discarded aromatic polymers such as PET and polycarbonates (PC) provide a viable raw material for the production of gasoline and, notably, aviation-fuel components, which require a mixture of aromatic and cycloalkane species (30-70 wt.%) to meet ASME jet-fuel requirements.[5-7] However, many aromatic polymers contain heteroatoms (e.g., O, N) within their structure, which inhibit their use as a fuel source, as jet fuel typically requires less than <0.5% oxygen content.[7, 8] Typically, high-pressure H_2 (> 20 bar) is required to deoxygenate the polymer products through catalytic hydrogenolysis.[9, 10]

In recent years, interest has grown in developing heterogenous catalysts to chemically "upcycle" PET at high H_2 pressures (> 50 bar) to produce valuable products (**Figure 1**), including aromatics and cycloalkanes.[1, 10-17] For example, Hongkailers *et al.* used a Co catalyst supported on titania (TiO_2) to convert PET to arenes, namely benzene, toluene, and xylene (BTX), with up to 79% yield, at 340 °C and 30 bar H_2 pressure (p_{H2} = 30 bar),[18] whereas Jing *et al.* converted various aromatic polymers, including PET and PC, to BTX over Ru/Nb_2O_5 at up to 83% yield in water (H_2O) at 200–280 °C and p_{H2} = 30 bar, where hydrolysis of PET and PC formed their monomeric units followed by hydrogenolysis of the monomers to BTX.[19]

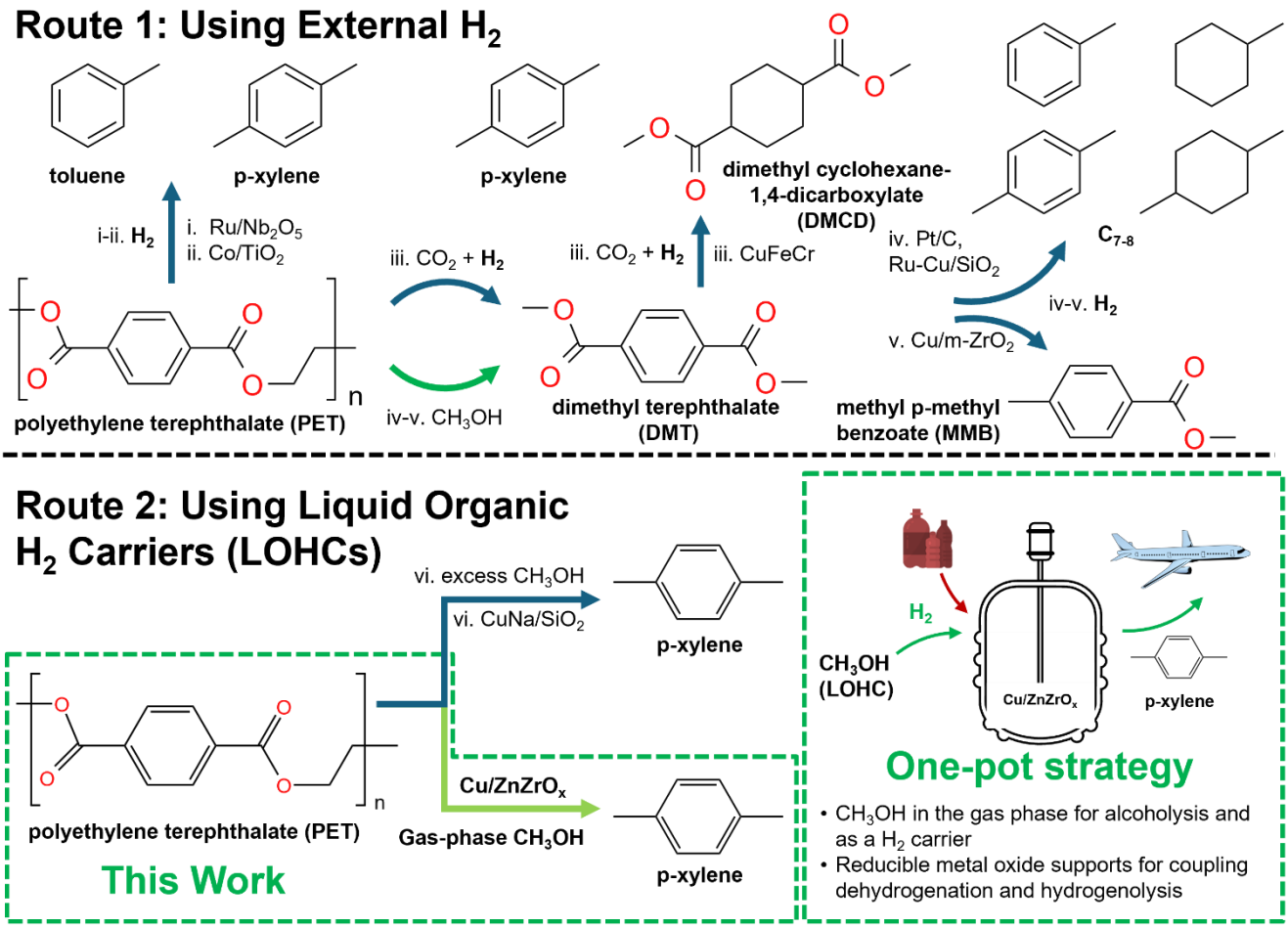

Figure 1. Routes for catalytically upcycling polyethylene terephthalate (PET) into aromatic and cycloalkanes. Route 1: Hydrogenolysis is conducted by supplying H_2 externally, either for a single-step conversion of PET (i and ii) or by alcoholysis to form dimethyl terephthalate (DMT) followed by its hydrogenolysis (methanol is generated *in situ* from CO_2 and H_2 via methanol synthesis in iii and is externally supplied in iv-v). Route 2: Methanol is used as a liquid organic hydrogen carrier (LOHC) for hydrogenolysis to supply H_2 internally via methanol dehydrogenation: vi. Uses a Cu-silicate catalyst, and our work uses the interface of Cu on reducible $ZnZrO_x$ at the catalytically active surface). Ref: i. Jing et al.[8], ii. Hongkaillers et al.[7], iii. Li et al.[11], iv. Tang et al.[10b], v. Cheng et al.[9], and vi. Gao et al.[14].

Further reports have utilized supported and promoted Cu catalysts to deoxygenate dimethyl terephthalate (DMT, the methyl ester of the PET monomer) to arenes and cycloalkanes under moderate temperatures (100-240 °C) and high p_{H2} (< 50 bar) after utilizing water (H_2O) or alcohols for the chemo(hydro- or alcohol-)lysis of PET to DMT. Recently, Cheng *et al.* utilized Cu supported on monoclinic zirconia (m-ZrO_2) for the hydrogenolysis of DMT to p–methyl benzoate with 86% selectivity at 160-200 °C and p_{H2} = 10 bar.[20] Tang *et al.* developed a cascading reaction sequence to depolymerize PET to DMT at ~97% yield and 200 °C with

excess methanol (CH_3OH) in the liquid-phase *via* methanolysis followed by solvent-free hydrogenation of the solid DMT over a Pt/C catalyst and concluded with a solvent-free hydrodeoxygenation over a Ru-Cu/SiO_2 catalyst at 100-140 °C and p_{H2} = 50 bar to form a mixture of deoxygenated C_7-C_8 aromatics and cycloalkanes in the gasoline and jet-fuel range.[21, 22] Interestingly, Li *et al.* demonstrated the use of CuFeCr layered double hydroxides (LDH) to simultaneously convert carbon dioxide (CO_2) and H_2 to CH_3OH, depolymerize PET to DMT via methanolysis, and deoxygenate DMT to p-xylene (PX) through hydrogenolysis at 240 °C at p_{H2} and p_{CO2} of 15 bar each.[23]

While the above studies have utilized high-pressure H_2, it is expensive and derived from fossil sources.[9] For example, in 2021, only 1% of H_2 was classified as low emissions.[9] As such, H_2-free routes are desired to deconstruct plastic wastes effectively and sustainably. H_2 is challenging to transport and store, opening the door for liquid organic hydrogen carriers (LOHCs), such as short-chain alcohols. For example, CH_3OH is the alcohol with the lowest molecular weight and a high-gravimetric H_2 content of 12.6 wt.% H_2.[24-26] However, effective catalysts must be able to simultaneously dehydrogenate the LOHCs and perform hydrogenolysis of PET and/or its monomers/oligomers to produce valuable fuels and platform chemicals. Recent works have utilized alcohols as H_2 sources for the cleavage of ester linkages (-(C=O)-OR) of PET and its monomer DMT. For instance, Lu *et al.* coupled *in-situ* ethylene glycol (EG) production from PET hydrolysis with reforming EG to form H_2 and then produced BTX over a Ru/Nb_2O_5 catalyst at 220 °C.[27] Gao *et al.* selectively converted PET to PX in a H_2-free one-pot method over Na-doped copper silicate catalyst in contact with CH_3OH in the liquid-phase at 210 °C.[28]

Notably, such studies have utilized excess alcohols in the liquid-phase for solvolysis. Interestingly, in a recent work, Bai *et al.* proposed the formation of a heterogenous Zn-layer at ~100 parts per million (ppm) to be crucial for the vapor-phase depolymerization of PET to DMT

at 160-180 °C for 2 h, at much lower temperatures than a commercial methanolysis process of 300 °C.[29] As such, this raises the question of whether such mild vapor-phase methanolysis of PET to DMT can be combined with the use of CH_3OH as a H_2 source to achieve a H_2-free one-pot upcycling of PET. In fact, Zeng *et al.* have shown that low amounts of CH_3OH in a batch reactor (likely leading to vapor-phase CH_3OH) as a H_2 source can depolymerize polystyrene (PS) to alkylbenzenes at 93% yield over Ru/SiO_2 catalyst at 280 °C, indicating the promise of this route.[30]

Evidently, the interfaces between Cu metal and supports have been linked to high activity for alcohol (especially CH_3OH) dehydrogenation and CH_3OH synthesis (from CO_2 and H_2) reactions, especially on Cu catalysts supported on ZnO or ZrO_2. The interfacial sites were suggested to play an important role in providing active sites for adsorption of CO_2 or CH_3OH, stabilizing key reaction intermediates such as formate species, and tuning reaction pathways (formaldehyde or CO/CO_2 formation from CH_3OH dehydrogenation).[31-34]

In the present work, we demonstrate the importance of the metal-support interface between Cu metal and a reducible metal oxide support, especially $ZnZrO_x$ (Zn/Zr ≈ 1/3.5) toward the dual-role played by CH_3OH for methanolysis and as a H_2-source. In a one-pot system, PET was converted to PX in a tandem sequence of vapor-phase methanolysis of PET to DMT, catalytic CH_3OH dehydrogenation to produce H_2, and the hydrogenolysis of DMT to PX (**Figure 1**). Furthermore, we demonstrate the crucial role of limiting liquid-phase components to reduce H-surface coverage due to destabilizing interactions of the condensed-phase environment. We perform pre- and post-reaction surface and bulk characterization along with *ab initio* density functional theory (DFT) computations to explicate the role of the metal-support interface for effective catalyst performance toward identifying the likely reaction pathways and providing a potential catalyst design framework for the upcycling of condensation polymers. We finally

extend the dual role played by CH_3OH for the alcoholysis and catalytic transfer hydrogenolysis (CTH) of waste PC polymers.

Results and Discussion

We first investigated the catalytic transfer hydrogenolysis (CTH) of dimethyl terephthalate (DMT), utilizing CH_3OH as a H_2-carrier (**Table 1**) on copper (Cu) metal (5 wt.%), supported on redox-inert silica (SiO_2) and reducible metal-oxides indium oxide (In_2O_3), ceria (CeO_2), titania (TiO_2) and mixed zinc zirconia ($ZnZrO_x$, Zn/Zr ≈ 1/3.5) at 240 °C for 16 h (3.5 g of dioxane was the solvent for effective carbon balances). BET surface areas and powder X-ray diffraction (PXRD) patterns are shown in **Table S1** and **Figures S1** and **S2**, respectively. The catalyst screening reactions are summarized in **Table S2**. Briefly, there was no DMT conversion observed on Cu/SiO_2. In contrast, among Cu supported on reducible metal-oxide supports, Cu/TiO_2 showed ~31% DMT conversion, while Cu/In_2O_3, Cu/CeO_2, and $Cu/ZnZrO_x$ showed complete conversion of DMT. The activity of supports alone (i.e., In_2O_3, CeO_2, $ZnZrO_x$) showed low to negligible DMT conversions (< 8%) under identical conditions, suggesting that the presence of Cu and its interface with the support was crucial for the catalyst activity. Notably, $Cu/ZnZrO_x$ showed the highest yields toward the completely deoxygenated product, p-xylene (PX, 97%), followed by Cu/CeO_2 (87%) and Cu/In_2O_3 (48%). Overall, these results suggest that the synergistic effects of Cu and the reducible metal oxide, plausibly at the metal-oxide interface, are crucial for CTH, i.e., the dehydrogenation of CH_3OH to form H_2 and its coupling with the hydrogenolysis (with H_2) of C-O bonds of DMT.

To investigate the underlying reasons for the observed reactivity, we next considered the gas-phase composition of the batch reactor at the conclusion of the reaction with Cu/SiO_2, $ZnZrO_x$, and $Cu/ZnZrO_x$ catalysts. (**Table 2**).

Table 1. Catalytic transfer hydrogenolysis (CTH) of dimethyl terephthalate (DMT) with methanol (CH_3OH) as a H_2-source in contact with the catalysts (Cu/SiO_2, Cu/TiO_2, In_2O_3, CeO_2, $ZnZrO_x$, Cu/In_2O_3, Cu/CeO_2, $Cu/ZnZrO_x$). Reaction conditions: 0.1 g DMT, 0.1 g catalyst, 3.5 g dioxane. 2 g methanol, 16 h, 30 bar initial N_2, 240 °C.

Catalyst[a]	DMT conversion (C-mol%)	Product yield (C-mol%)		Carbon balance[b] (mol%)
		p-xylene	methyl p-toluate	
Cu/SiO_2	0%	0%	0%	106%
Cu/TiO_2	31%	1%	24%	103%
In_2O_3	0%	0%	0%	112%
Cu/In_2O_3	100%	48%	39%	88%
CeO_2	8%	0%	2%	105%
Cu/CeO_2	100%	87%	1%	96%
$ZnZrO_x$	1%	0%	1%	108%
$Cu/ZnZrO_x$	100%	97%	0%	102%

Interestingly, on Cu/SiO_2 and $ZnZrO_x$, the negligible DMT conversion was concomitant with the negligible post-reaction formation of H_2 (from CH_3OH dehydrogenation). In contrast, for $Cu/ZnZrO_x$, the gas-phase composition showed that ~21 mol% of the total gas-phase comprised of H_2. Taken together, our data suggests that the Cu and the $ZnZrO_x$ support alone were not responsible for CH_3OH dehydrogenation to H_2. In fact, we can infer that the metal-support interface of Cu metal and $ZnZrO_x$ support was likely responsible for the CH_3OH dehydrogenation

and the concomitant DMT hydrogenolysis to PX under our reaction conditions. Notably, we confirmed the reproducibility of this highly selective transfer hydrogenolysis of DMT to PX over 4 separate runs (**Table S3**).

To confirm the role of CH_3OH in supplying H_2, we performed DMT hydrogenolysis with p_{H2} = ~10 bar in the absence of CH_3OH, corresponding to the final H_2 concentration (~21% in the gas-phase) at the end of the reaction, and determined that the PX yields were similar (91% compared to 97% at 16 h, see **Table S4**). In **Table S4**, we have summarized the final PX yields and H_2 concentrations from the hydrogenolysis of (1) PET using H_2 generated in-situ from CH_3OH dehydrogenation and (2) DMT using both in-situ generated H_2 and external H_2. We note that the similar trends for final H_2 concentrations and PX yields further confirmed that the H_2 for hydrogenolysis indeed originated from the dehydrogenation of CH_3OH (**Figure S6**).

Table 2. Catalytic transfer hydrogenolysis (CTH) of dimethyl terephthalate (DMT) with methanol (CH_3OH) in contact with catalysts (Cu/SiO_2, $ZnZrO_x$, $Cu/ZnZrO_x$). Reaction conditions: 0.1 g DMT, 0.1 g catalyst, 3.5 g dioxane. 2 g methanol, 16 h, 30 bar initial N_2, 240 °C.

Catalyst[a]	DMT conversion (C-mol%)	Product yield (C-mol%)		Carbon balance[b] (mol%)	Gas increase (mol%)	Final H_2 gas concentration (mol%)	Gas mole balance[c] (mol%)
		p-xylene	methyl p-toluate				
Cu/SiO_2	0%	0%	0%	106%	5%	3%	100%
$ZnZrO_x$	1%	0%	1%	108%	2%	0%	102%
$Cu/ZnZrO_x$	100%	97%	0%	102%	76%	21%	98%

[a] Cu loading of 5wt.%.[b] Carbon-balance was made on the aromatic PET content pre- and post-reaction.[c] Gas-mole balance is done with respect to total moles of gas moles post-reaction based on the ideal gas law and GC detected gases.

We next investigated whether the nature of the interface between the catalyst and the reaction medium (between CH_3OH, H_2, and the catalyst surface) plays a role in DMT hydrogenolysis reactivity (**Figure 1**), i.e., whether the liquid- or vapor-phase CH_3OH was critical for the reaction. To investigate this, we varied the initial amount of CH_3OH in the batch reactor. Notably, the PX yield reduced drastically from ~70% to 20% and finally 0% as the initial CH_3OH amount was increased from 2 g to 4 g and finally 8 g (**Figure 2A**). Interestingly, the final gas-phase H_2 concentration was 20-22 mol % irrespective of the initial CH_3OH amount, implying that differences in CH_3OH dehydrogenation rates were not the reasons contributing to the decreased PX yields and DMT hydrogenolysis rates.

The question next arises whether changing the initial CH_3OH amount leads to a change in the reactor phase-composition or if the increased CH_3OH amount leads to competitive adsorption between DMT and CH_3OH, as the concentration of CH_3OH under reaction conditions may increase with the increasing initial CH_3OH amount. The free-energy of adsorption of CH_3OH and DMT-analogue *(vide infra)* at the metal-support interfacial active sites at 513 K (i.e., the reaction temperature) was 18 kJ/mol and -25 kJ/mol, respectively, (estimated with density functional theory (DFT) computations) suggesting that the reduced DMT conversion was likely not due to more favorable adsorption of CH_3OH at the interfacial active sites. We, therefore, infer that the CH_3OH phase is likely the reason for the observed inhibition of hydrogenolysis activity. We investigated this by estimating the phase composition of the reactor under reaction conditions (using a calculated average reactor temperature, see **Figure S3**) utilizing ASPEN Plus simulations (**Figure 2B**). Under reaction conditions, it is notable that the mass of the liquid-phase increased from ~0.2 g to ~0.3 g, and ~2.7 g (for the three different initial CH_3OH),

comprising ~4%, ~3%, and ~23% of the initial liquid. Notably, ~2% of initial CH_3OH (and ~5% of initial dioxane) remained in the liquid phase with 2 and 4 g of initial CH_3OH load, while ~20% of initial CH_3OH (and ~40% of dioxane) remained in the liquid-phase with a ~8 g of initial CH_3OH amount. As such, the catalyst was likely in contact with the condensed phase with the high 8 g initial CH_3OH amount.

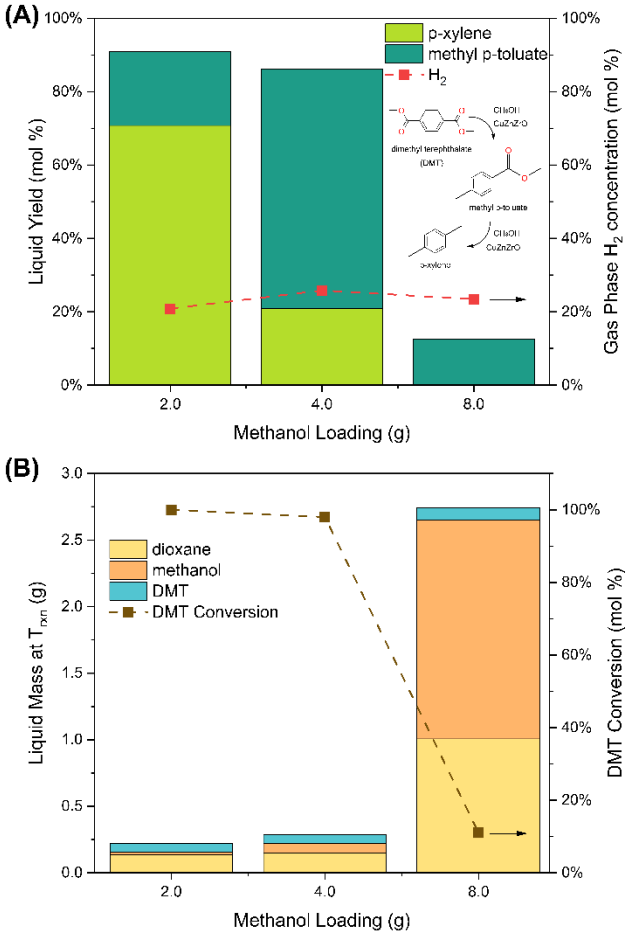

Figure 2. (a) Effect of initial methanol amount in the batch-reactor on p-xylene and methyl p-toluate yields (left y-axis) and H_2 concentration in the gas-phase (right y-axis). (b) Liquid phase composition in the batch reactor (left y-axis) and DMT conversion (right y-axis). Reaction conditions: 0.1 g PET, 0.1 g $Cu/ZnZrO_x$, 3.5 g dioxane. 2-8 g methanol, 16 h, 30 bar initial N_2, 240 °C.

While the H_2 concentration in the gas-phase was largely invariant with varying initial CH_3OH amounts, the chemical potential of surface H and, consequently, the H-surface coverage on the catalyst was likely substantially reduced due to destabilizing interactions of the surface H with the condensed phase. Recent work by Lercher and coworkers has shown that condensed-phase CH_3OH reduced surface H-coverage on supported-Pd catalysts, primarily due to the destabilizing solvation of adsorbed surface H at the catalyst solid-liquid interface as compared to the catalyst solid-gas interface in the absence of the solvent.[35] As such, the catalyst contact with gas-phase H_2 was likely critical for high DMT hydrogenolysis rates. This was achieved by utilizing vapor-phase CH_3OH rather than in the condensed-phase (achievable under the low initial CH_3OH amount).

We next investigated the sequential chemolysis of PET to DMT (with CH_3OH in the vapor-phase) and catalytic transfer hydrogenolysis (CTH) of DMT to methyl p-toluate and PX **(Figure 2)** at 240 °C from 0 – 24 h in contact with $Cu/ZnZrO_x$. We note that each data point represents an independent experiment. First, we observed a fast conversion of PET to DMT (~90% yield) within 2 h, followed by a gradual reduction of PET yield to below 5% after 12 h. The hydrogenolysis of PET was ruled out as we did not observe any terephthalic acid (TPA), the hydrogenolysis product, at any time during the reaction. DMT yields gradually dropped from ~90% to ~75% from 2 – 8 h, concomitant with an increase in yields of methyl p-toluate from 0 to 17% in the same time period. After 8 h, DMT yields dropped drastically from 75% to less than 5% between 8 – 12 h, concomitant with an increase in methyl p-toluate yields from ~17% to 50% and PX yields from 0% to ~35%. Between 12 – 24 h, methyl p-toluate yields decreased from ~50% to ~10%, while PX yields increased from ~35% to ~70%. In addition to the major products, PX and methyl p-

toluate, alkylated benzenes were observed as minor products (see **Figure S4**). Interestingly, we did not observe methyl 4-(hydroxymethyl)benzoate and 4-methyl benzyl alcohol intermediates, suggesting they were short-lived reaction intermediates due to the fast hydrogenolysis of alcohols, consistent with previous work by Gao et al. on copper silicate ($CuSiO_3/SiO_2$) catalysts.[28]

Crucially, the H_2 fraction in the gas-phase increased from 0 – 17% from 0 – 12 h (from CH_3OH dehydrogenation, **Figure S5**) and then gradually increased from 17 – 22% from 12 – 24 h. This increase in H_2 evolution was consistent with the increased yields of the hydrogenolysis products, methyl p-toluate and PX (**Figure S6**). A control reaction of CH_3OH dehydrogenation (in the absence of DMT) leads to ~25% H_2, compared to ~21% in the presence of DMT and ~17% in the presence of PET at 16 h. We tracked the reactor pressure over time (2-24 h) for each of these reactions (**Figure S7**), which revealed that the evolution of gas-phase and volatile products followed a similar trend, confirming that the hydrogenolysis followed a sequential path **(Figure 3B)**. We hypothesize that the PET first undergoes complete methanolysis, forming DMT, followed by the sequential hydrogenolysis of its ester groups, first forming mono-methyl terephthalate (MMT), followed by methyl-p-toluate, toluic acid, and finally PX. The proposed hydrogenolysis reaction pathway is presented in **Figure S8**.

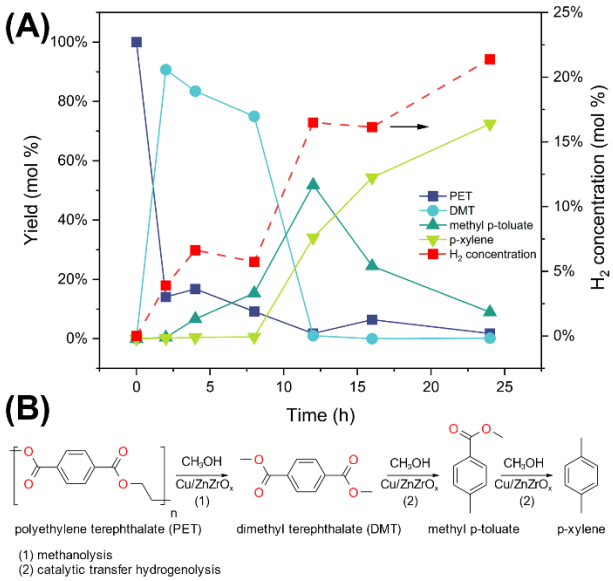

Figure 3. Time evolution of products from polyethylene terephthalate (PET) solvolysis for the formation of dimethyl terephthalate (DMT) and catalytic transfer hydrogenation (CTH) of DMT to form methyl p-toluate and p-xylene. Reaction conditions: 0.1 g PET, 0.1 g $Cu/ZnZrO_x$, 3.5 g dioxane. 2 g methanol, 16 h, 30 bar initial N_2, 240 °C.

After 8 h, DMT yields dropped drastically from 75% to less than 5% between 8 – 12 h, concomitant with an increase in methyl p-toluate yields from ~17% to 50% and PX yields from 0% to ~35%. Between 12 – 24 h, methyl p-toluate yields decreased from ~50% to ~10%, while PX yields increased from ~35% to ~70%. In addition to the major products, PX and methyl p-toluate, alkylated benzenes were observed as minor products (see **Figure S4**). Interestingly, we did not observe methyl 4-(hydroxymethyl)benzoate and 4-methyl benzyl alcohol intermediates, suggesting they were short-lived reaction intermediates due to the fast hydrogenolysis of alcohols, consistent with previous work by Gao et al. on copper silicate ($CuSiO_3/SiO_2$) catalysts.[28]

Crucially, the H_2 fraction in the gas-phase increased from 0 – 17% from 0 – 12 h (from CH_3OH dehydrogenation, **Figure S5**) and then gradually increased from 17 – 22% from 12 – 24 h. This increase in H_2 evolution was consistent with the increased yields of the hydrogenolysis products, methyl p-toluate and PX (**Figure S6**). A control reaction of CH_3OH dehydrogenation (in the absence of DMT) leads to ~25% H_2, compared to ~21% in the presence of DMT and ~17% in the presence of PET at 16 h. We tracked the reactor pressure over time (2-24 h) for each of these reactions (**Figure S7**), which revealed that the evolution of gas-phase and volatile products followed a similar trend, confirming that the hydrogenolysis followed a sequential path **(Figure 3B)**. We hypothesize that the PET first undergoes complete methanolysis, forming DMT, followed by the sequential hydrogenolysis of its ester groups, first forming mono-methyl terephthalate (MMT), followed by methyl-p-toluate, toluic acid, and finally PX. The proposed hydrogenolysis reaction pathway is presented in **Figure S8**.

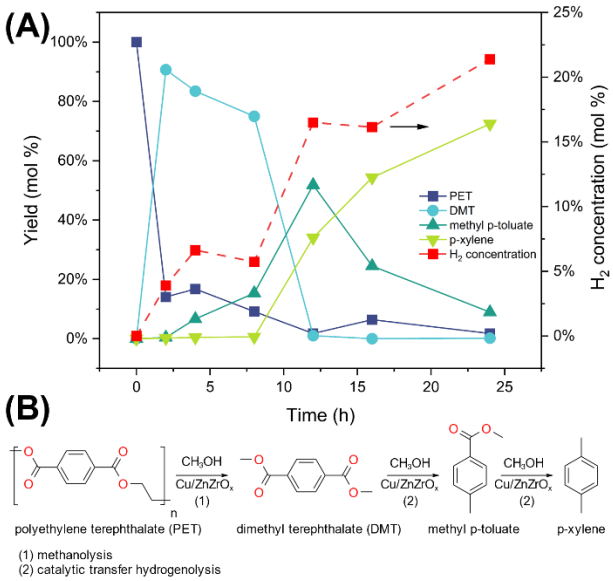

Figure 4. Time evolution of products from polyethylene terephthalate (PET) solvolysis for the formation of dimethyl terephthalate (DMT) and catalytic transfer hydrogenation (CTH) of DMT to form methyl p-toluate and p-xylene. Reaction conditions: 0.1 g PET, 0.1 g $Cu/ZnZrO_x$, 3.5 g dioxane. 2 g methanol, 16 h, 30 bar initial N_2, 240 °C.

To probe the crucial role played by the metal-support interfaces, we investigated the reducibility of the $Cu/ZnZrO_x$ catalysts in comparison with the $ZnZrO_x$ support and Cu/SiO_2 by hydrogen temperature programmed reduction (H_2-TPR) and electron paramagnetic resonance (EPR) spectroscopy on reduced catalysts (at 450 °C with 10% H_2, see Supporting Information, **S2**, for detailed information). H_2-TPR of $ZnZrO_x$ (**Figure 4A**) showed a broad high-temperature H_2 consumption peak (0.15 mmol H_2/g_{cat}) with a peak temperature of ~580 ˚C, likely associated with the production of oxygen vacancies.[36] Cu/SiO_2 shows a broad H_2-consumption peak (1.12 mmol H_2/g_{cat}) with a peak temperature of ~250 °C and a H_2 consumption corresponding to $H_2/Cu \approx 1.4$, suggesting that the H_2 consumption was associated with the reduction of CuO (Cu^{2+}) to Cu (Cu^0)

metal. In comparison, Cu/$ZnZrO_x$ showed two peaks of H_2 consumption (peak temperatures of 155 °C and 210 °C) and a H_2 consumption corresponding to H_2/Cu = 2.5, suggesting an ease of reduction of Cu species on $ZnZrO_x$ support compared to SiO_2. In addition, the higher H_2 consumption suggests the easier reduction of the $ZnZrO_x$ support on the deposition of Cu on the support. This was further confirmed with EPR spectroscopy of the reduced catalysts (**Figure 4B**). Specifically, the $ZnZrO_x$ sample showed a signal at a g factor of 2.08, likely attributed to Zr^{3+}, with one unpaired d electron.[37] Cu/SiO_2 showed a signal at a g factor of 2.14, likely associated with paramagnetic Cu^{2+} moieties.[38-40]

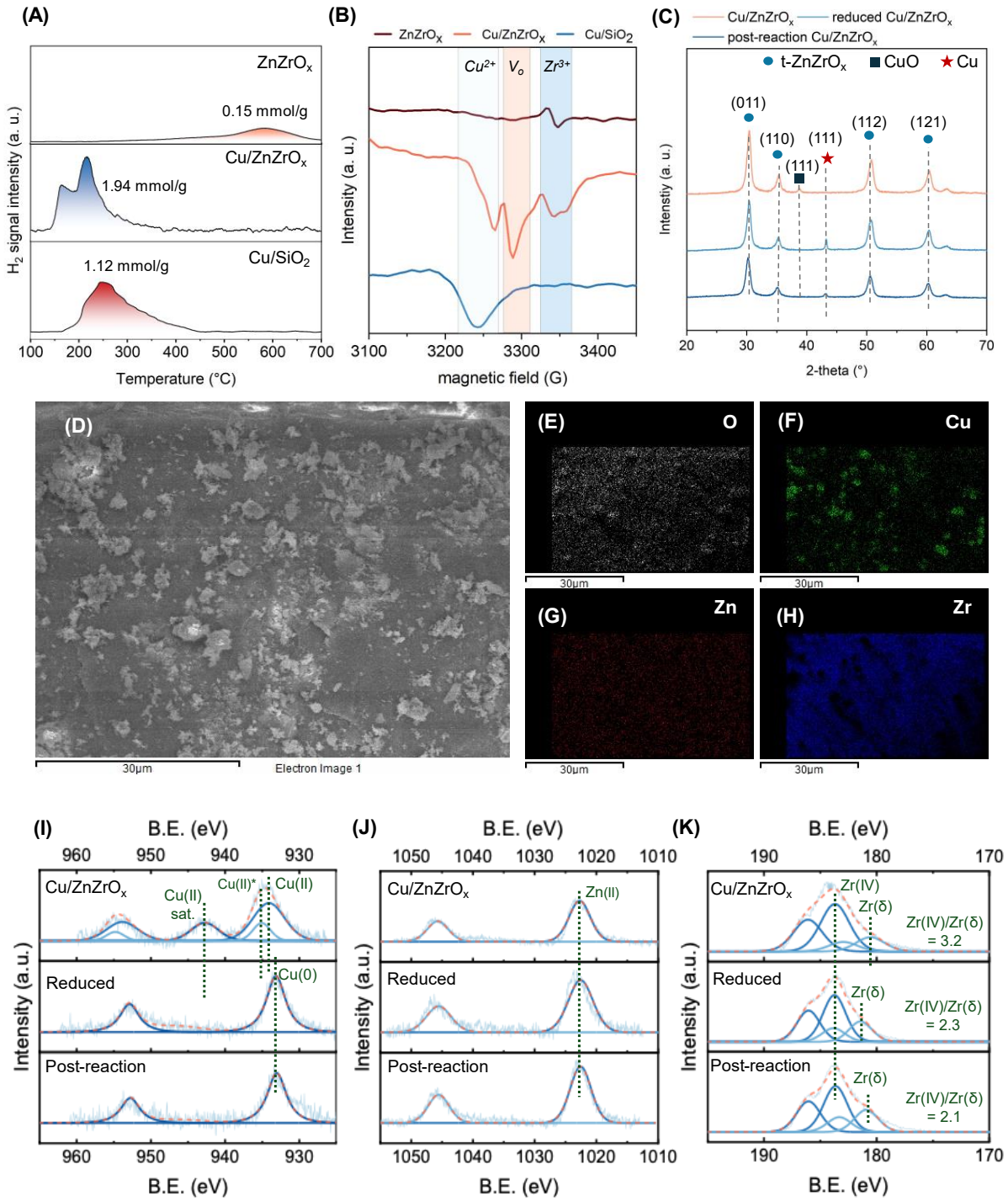

Figure 5. Characterization of Cu/ZnZrO$_x$ catalyst and ZnZrO$_x$ support. (A) Hydrogen temperature-programed reduction (H_2-TPR) of ZnZrO$_x$, Cu/SiO_2, and Cu/ZnZrO$_x$ catalysts. (B) Electron paramagnetic resonance (EPR) spectroscopy of reduced ZnZrO$_x$, Cu/SiO_2, and Cu/ZnZrO$_x$. (C) Powder X-ray diffraction (PXRD) patterns of Cu/ZnZrO$_x$, reduced Cu/ZnZrO$_x$, and post-reaction Cu/ZnZrO$_x$ catalysts. (E) SEM image and EDS maps (E-H) of Cu/ZnZrO$_x$. X-ray photoelectron spectroscopy (XPS) of (I) Cu 2p region and (J) Zn 2p region and (K) Zr 3d region.

Interestingly, Cu/ZnZrO$_x$ showed signals for the presence of both Cu^{2+} and Zr^{3+} with a g

factor of 2.13 and 2.08, respectively, with an additional peak with a g factor of 2.11. We infer that this additional peak could be associated with paramagnetic defects and the formation of oxygen vacancy sites, V_o, with an unpaired electron. This observation is consistent with the findings from H_2-TPR. Additionally, the peak area of Cu^{2+} reduced and shifted to a higher magnetic field in $Cu/ZnZrO_x$, which could be caused by the reduction of Cu^{2+} to diamagnetic Cu^0, consistent with H_2-TPR data showing a more facile reduction of $Cu/ZnZrO_x$ compared to Cu/SiO_2. The bulk and surface properties of the $Cu/ZnZrO_x$ catalyst were next interrogated with powder X-ray diffraction (PXRD) patterns (**Figure 4C**) and X-ray photoelectron spectroscopy (XPS) of pre-reaction, reduced, and post-reaction samples (**Figure 4I-K**). PXRD patterns of the catalyst pre-reaction showed the $ZnZrO_x$ support to be of tetragonal phase and showed no formation of ZnO, suggesting the support to be a Zn-Zr solid solution. The peaks at 2Θ of 38.86° correspond to the (111) facet of CuO. Scanning electron microscopy (SEM) of fresh $Cu/ZnZrO_x$ (**Figure 4D-H**) showed distinct locations of Cu and Zr, suggesting the deposition of Cu on the support and the absence of any Cu-containing mixed-metal oxide phase. SEM images of the support $ZnZrO_x$ are shown in **Figure S9**. In samples post-reduction and post-reaction, the

peaks corresponding to the support appeared to be unaffected, with new peaks at 2Θ value of 43.26°, corresponding to the (111) facet of Cu metal.

Figure 4I-K shows the XP spectra of Cu 2p, Zn 2p, and Zr 3d regions for the Cu/$ZnZrO_x$ catalyst pre-reaction, reduced (450°C for 3 h), and post-reaction (of the reduced catalysts). The Cu 2p spectra (**Figure 4I**) indicates that pre-reduction Cu species exist exclusively as Cu(II), as evidenced by the prominent Cu(II) satellite feature at ~942 eV. Following reduction and reaction, the Cu species are reduced to Cu(0), as indicated by a downward shift in binding energy to 933.1 eV, consistent with PXRD patterns. We note that in the absence of a weak satellite feature around 946 eV peak, we excluded the

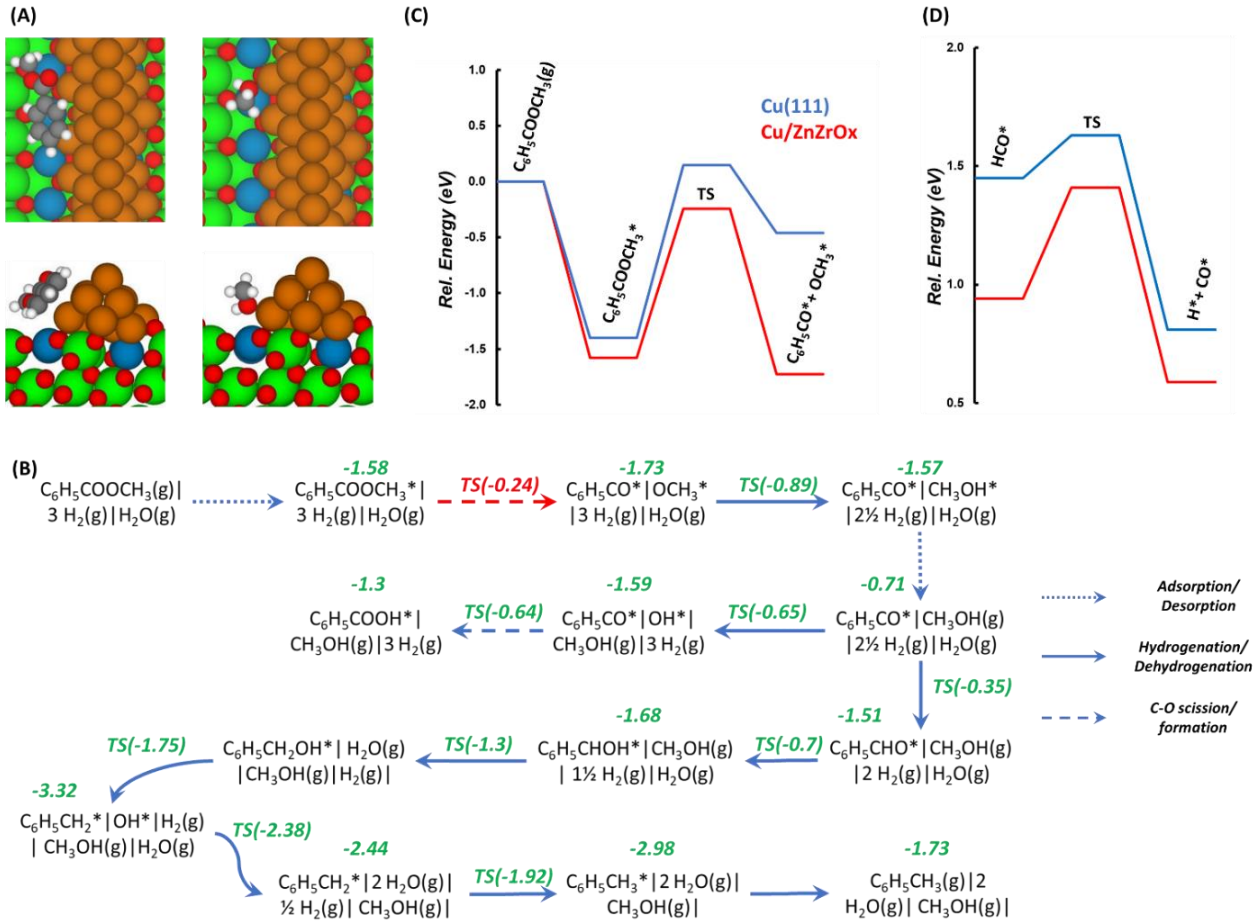

Figure 6. (A) The top and side views of the catalyst model for $Cu/ZnZrO_x$ catalyst with methyl benzoate (left) and methanol (right) adsorbed at the metal-support interface. Cu atoms are in orange, Zn atoms in blue, Zr in green, O in red, C in grey, and H in white. (B) The reaction pathways and associated DFT energetics of methyl benzoate hydrolysis to adsorbed benzoic acid ($C_6H_5COOH^*$) and hydrogenolysis to toluene on $Cu/ZnZrO_x$ catalyst interface. (C) The energetics of the plausible rate-controlling step for methyl benzoate conversion on $Cu/ZnZrO_x$ shown in red in (B) and the corresponding energies on Cu(111). (D) The energetics of the plausible rate-controlling step for methanol decomposition to CO on $Cu/ZnZrO_x$ and the corresponding energies on Cu(111). The relative energy of the species and transition states (TSs) in (B) are given with respect to methyl benzoate, 3 molecules of H_2, and H_2O. The activation barrier (not shown) for each step in (B) is the difference in the energy of its TS and initial state (IS) while the reaction energy is the difference between final state (FS) and IS. Each state in (B) has the same number of atoms and co-adsorbed and infinitely separated species are demarcated by "+" and "|" respectively. All energies in (B)-(D) are in eV. Characterization of $Cu/ZnZrO_x$ catalyst and $ZnZrO_x$ support.

possibility of partially oxidized Cu(I) species. To probe whether the support undergoes a similar reduction to the Cu catalyst, the Zn 2p region was analyzed. Interestingly, as shown in **Figure 4J**, Zn does not appear to undergo a reduction as a single peak was present at 1022.5 eV, which is assigned to Zn(II) species. Additionally, the Zr 3d region (**Figure 4K**) showed a prominent peak at 183.7 eV for all samples, which was assigned to Zr(IV) species, and peaks associated with Zr sub-oxide species (denoted as Zr(δ)), which are likely associated with oxygen vacancies or Zr(III) moieties. Interestingly, the ratio of the Zr(IV) peak to the Zr(δ) reduced for the samples upon reduction and post-reaction, indicating an increase in oxygen vacancies upon reduction and post-reaction. This is consistent with the increase in oxygen vacancy concentrations suggested by EPR on reduced catalysts and H_2-TPR (**Figure 4A-B**). XP spectra of the Zn 2p and Zr 3d regions are shown in **Figures S10 and 11**.

DFT calculations (details in the Supplementary Information, **S5**) were carried out on a Cu nanorod model on tetragonal $ZrO_2(101)$ with some Zr atoms in the first and second row of the slab replaced by Zn (as determined from thermochemistry but following a Zn:Zr of 1:3, which is close to the experimental composition). This is consistent with the

nanoparticles of Cu metal detectable via PXRD and Cu deposition on the support observed via SEM, allowing the study of the metal-oxide interface and reactions on these sites (**Figure 5A, Figure S13**). Replacing Zr atoms by Zn requires removing oxygen atoms to maintain the correct stoichiometry. Further removal of oxygen atoms as water (by one H_2 molecule) in a stoichiometric slab was thermoneutral. These results confirm the experimental observation of higher oxygen vacancy on this surface and a larger H_2/Cu value in H_2-TPR. A Cu(111) model was also simultaneously studied to mimic the Cu/SiO_2 catalyst.

Methyl benzoate and benzoic acid were used to model the carboxyl (-C(=O)O-) functional group of DMT. The acid (-1.43 eV), ester (-1.58 eV), and methanol (-0.86 eV) prefer binding at the interface of Cu/$ZnZrO_x$ (**Figure 5A** and **Figures S18 and S19**); the large binding strength of the ester and acid indicates significant dispersion stabilization due to the aromatic group. **Figure 5B** shows the reaction network and energetics of the most energetically favored pathway for methyl benzoate conversion to toluene, while **Figure S14** shows the entire hydrogenolysis network (comprising alternative pathways) using benzoic acid as the model compound. The scission of the ester C-O linkage (**Figure 5B**) to form C_6H_5CO* and OCH_3* is the step with the highest transition state (TS) energy (having a relative energy of -0.24 eV with respect to gaseous initial states and corresponding to an activation barrier of 1.34 eV for the scission step). This plausibly indicates that the first C-O scission of the ester is rate controlling.

Similarly, the dissociation of the C-OH bond of the acid is rate-controlling (**Figure S14**). The resulting carbonyl species (C_6H_5CO*) then undergoes successive hydrogenation to form $C_6H_5CH_2OH$*; and subsequent C-O scission results in the precursor $C_6H_5CH_2$* which

then gets hydrogenated to toluene. The steps after the first C-O scission are likely fast, explaining the absence of partially hydrogenated/hydrogenolyzed intermediates in experiments (**Figure 3**). While the chemistry is similar on Cu(111) (see **Figure S15** for the energetics of the partial network of methyl benzoate hydrogenolysis), the relative energies (and barriers) are significantly higher than at the interface. Specifically, the relative energy of the TS of the ester C-O dissociation step is 0.39 eV higher on Cu(111) than on $Cu/ZnZrO_x$ (**Figure 5C**), clearly indicating the role of the interface in the latter. DFT calculations on $Cu/ZnZrO_x$ and Cu(111) of CH_3OH decomposition to CO (and subsequent water gas shift reaction to produce H_2 and CO_2) also show more favorable energetics (**Figure 5D**) on the interfacial sites (see **Figures S16 and S17** for the corresponding potential energy surfaces and **Figures S20 and S21** for the structures). Indeed, the rate-determining TS of methanol dissociation on $Cu/ZnZrO_x$, viz., C-H dissociation of HCO*, is 0.22 eV more stable than the corresponding step on Cu(111). This is in line with the observation of a higher H_2 yield on $Cu/ZnZrO_x$ relative to Cu/SiO_2. Overall, our DFT calculations show the critical role of the interface in adsorbing CH_3OH and the PET monomer.

We finally investigated the broad applicability of the one-pot solvolysis and catalytic transfer hydrogenolysis strategy for bisphenol A polycarbonates (BPA-PC), another ubiquitous condensation polymer (**Figure 6**). Specifically, we contacted PC with $Cu/ZnZrO_x$ under identical reactions (240 °C for 16 h) as PET. Interestingly, while this strategy for PET yielded the deoxygenated products (i.e., showed C-O bond hydrogenolysis), methyl p-toluate, and PX, PC exhibited full conversion and C-C bond hydrogenolysis and methylation of the monomer to yield xylenol and isopropyl methyl

anisole as dominant products (at yields 37 C-mol% and 45 C-mol%, respectively, **Figure 6B**). We confirmed that the methylation was the primary reason for the formation of alkylated phenols and anisoles by performing a ^{1}H-nuclear magnetic resonance (NMR) spectroscopy (**Figure S12**) of the BPA-PC substrate, which showed that there were no alkyl groups present on the aromatic rings of the initial polymer (**Figure S4** shows the chromatogram of the liquid products formed from the BPA-PC substrates and **Table S6** shows the carbon balance of the reaction). Evidently, the $C_{aromatic}$-O bond cleavage of the substituted phenol and anisole was harder, in line with the reported difficulty in C-O bond hydrogenolysis of phenolic (-$C_{aromatic}$-OH) bonds for biomass-derived compounds.[41, 42] Nonetheless, the data shows the promise of the strategy toward depolymerization of condensation polymers and the promise of the H_2-free strategy to deconstruct polycondensation polymers.

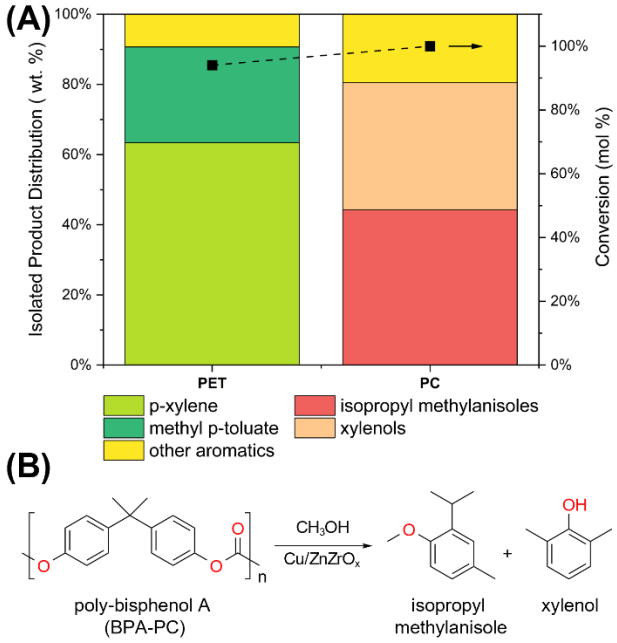

Figure 7. (A) One-pot solvolysis and catalytic transfer hydrogenolysis (CTH) of polyethylene terephthalate (PET) and polycarbonate (PC) polymers with methanol, and

(B) Schematic of PC conversion to isopropyl methyl anisole and xylenol. Reaction conditions: 0.1 g DMT, 0.1 g Cu/$ZnZrO_x$, 3.5 g dioxane. 2 g methanol, 16 h, 30 bar initial N_2, 240 °C.

Conclusion

In this work, we have demonstrated a one-pot, H_2-free strategy to convert polyethylene terephthalate (PET) to p-xylene (PX) using methanol to combine (1) the methanolysis of PET to dimethyl terephthalate (DMT) and (2) the catalytic transfer hydrogenolysis (CTH) of DMT to PX over a Cu supported on $ZnZrO_x$ catalyst with the H_2 generated in-situ from CH_3OH dehydrogenation. We showed the significant role played by vapor-phase CH_3OH in stabilizing surface H by controlling the phase composition of the reaction environment in the batch-reactor through the control of initial CH_3OH amounts. Density functional theory (DFT) calculations and bulk and surface characterization revealed that the interface between Cu and the reducible $ZnZrO_x$ support is critical for enabling the catalytic transfer hydrogenolysis (CTH) (i.e., coupling of CH_3OH dehydrogenation and DMT hydrogenolysis), by showing the relatively facile formation of oxygen vacancies on Cu/$ZnZrO_x$, interfacial sites for the adsorption of both CH_3OH and DMT and a low-energy pathway for C-O bond hydrogenolysis, as compared to Cu on a redox-inert SiO_2 support. DFT calculations showed that the rate-determining step was the cleavage of PET ester linkages (-(C=O)-OR). Finally, the one-pot solvolysis and CTH strategy was also effective in converting a BPA-polycarbonate (PC) substrate into xylenol and isopropyl methyl anisole via C-C bond hydrogenolysis compared to C-O bond hydrogenolysis for PET, promising a wider applicability of the one-pot strategy for the conversion of end-of-use condensation polymers. The CTH strategy demonstrates a pathway to convert plastic

wastes to sustainable fuels effectively and highlights the potential use of liquid organic hydrogen carriers (LOHCs) for upcycling of plastics.

Supporting Information

The authors have cited additional references within the Supporting Information.[43-56]

Acknowledgements

We acknowledge start-up support by Artie McFerrin Department of Chemical Engineering and the College of Engineering at Texas A&M University and Texas A&M Engineering Experiment Station (TEES). F.M. acknowledges support by the National Science Foundation (NSF) CBET grant number 2245474. J.V. acknowledges support from Dr. Dionel E. Avilés '53 and Dr. James E. Johnson '67 Graduate Fellowship at the Texas A&M University and the NSF Graduate Research Fellowship for support. M.M.F.H gratefully acknowledges partial support from the NSF CDS&E grant 2245474, NSF EFRI DCheM grant 2029354, and NSF CAREER grant CBET-1943479. A.I. acknowledges support from the Phillips 66 Technical Fellowship. S.R. acknowledges support by the NSF CAREER grant (CBET 2045550). The DFT calculations were conducted on Lehigh University's Research Computing infrastructure partially supported by National Science Foundation (NSF) grant 2019035, as well as Expanse at the San Diego Supercomputer Center (SDSC) and Stampede2 at Texas Advanced Computing Center through allocation CTS170035 from the Advanced Cyberinfrastructure Coordination Ecosystem: Services & Support (ACCESS) program, which is supported by NSF grants number 2138259, 2138286, 2138307, 2137603, and 2138296. The authors would like to thank the Xie

group for assistance with ^{1}H NMR experiments. The authors acknowledge the Texas A & M University Materials Characterization Core Facility (RRID:SCR_022202) for XPS and SEM data. The authors also acknowledge Dr. Hae-Kwon Jeong's group at TAMU for helping collect PXRD data.

Keywords: waste valorization • hydrogen transfer • supported catalysts • heterogeneous catalysis • condensation polymers

References

(1) Borkar, S. S.; Helmer, R.; Mahnaz, F.; Majzoub, W.; Mahmoud, W.; Al-Rawashdeh, M. m.; Shetty, M. Enabling resource circularity through thermo-catalytic and solvent-based conversion of waste plastics. *Chem Catalysis* **2022**, *2* (12), 3320-3356. DOI: https://doi.org/10.1016/j.checat.2022.09.003.
(2) MacLeo, M.; Arp, H. P. H.; Tekman, M. B.; Jahnke, A. The global threat from plastic pollution. *Science* **2021**, *373* (6550), 61-65. DOI: 10.1126/science.abg5433.
(3) Stubbins, A.; Law, K. L.; Muñoz, S. E.; Bianchi, T. S.; Zhu, L. Plastics in the Earth system. *Science* **2021**, *373* (6550), 51-55. DOI: doi:10.1126/science.abb0354.
(4) Nielsen, T. D.; Hasselbalch, J.; Holmberg, K.; Stripple, J. Politics and the plastic crisis: A review throughout the plastic life cycle. *Wires Energy Environ* **2020**, *9* (1). DOI: ARTN e360. 10.1002/wene.360.

(5) Edwards, J. T. Reference jet fuels for combustion testing. In *55th AIAA aerospace sciences meeting*, 2017; p 0146.
(6) Hadaller, O.; Johnson, J. *World fuel sampling program*; Coordinating Research Council, Incorporated, 2006.
(7) Stone, M. L.; Webber, M. S.; Mounfield, W. P.; Bell, D. C.; Christensen, E.; Morais, A. R. C.; Li, Y. D.; Anderson, E. M.; Heyne, J. S.; Beckham, G. T.; Román-Leshkov, Y. Continuous hydrodeoxygenation of lignin to jet-range aromatic hydrocarbons. *Joule* **2022**, *6* (10), 2324-2337. DOI: 10.1016/j.joule.2022.08.005.
(8) Products, A. C. D. o. P.; Lubricants. *Standard specification for aviation turbine fuel containing synthesized hydrocarbons*; ASTM International, 2014.
(9) Hancock, J. N.; Rorrer, J. E. Hydrogen-free catalytic depolymerization of waste polyolefins at mild temperatures. *Applied Catalysis B: Environmental* **2023**, *338*, 123071. DOI: https://doi.org/10.1016/j.apcatb.2023.123071.
(10) Rorrer, J. E.; Beckham, G. T.; Roman-Leshkov, Y. Conversion of Polyolefin Waste to Liquid Alkanes with Ru-Based Catalysts under Mild Conditions. *JACS Au* **2021**, *1* (1), 8-12, Article. DOI: 10.1021/jacsau.0c00041.
(11) Borkar, S. S.; Helmer, R.; Panicker, S.; Shetty, M. Investigation into the Reaction Pathways and Catalyst Deactivation for Polyethylene Hydrogenolysis over Silica-Supported Cobalt Catalysts. *ACS Sustain. Chem. Eng.* **2023**, *11* (27), 10142-10157. DOI: 10.1021/acssuschemeng.3c02202.
(12) Celik, G.; Kennedy, R. M.; Hackler, R. A.; Ferrandon, M.; Tennakoon, A.; Patnaik, S.; LaPointe, A. M.; Ammal, S. C.; Heyden, A.; Perras, F. A.; Pruski, M.; Scott, S. L.; Poeppelmeier, K. R.; Sadow, A. D.; Delferro, M. Upcycling Single-Use Polyethylene into High-Quality Liquid Products. *Acs Central Sci* **2019**, *5* (11), 1795-1803, Article. DOI: 10.1021/acscentsci.9b00722.
(13) Kots, P. A.; Liu, S.; Vance, B. C.; Wang, C.; Sheehan, J. D.; Vlachos, D. G. Polypropylene Plastic Waste Conversion to Lubricants over Ru/TiO2 Catalysts. *Acs Catal* **2021**, *11* (13), 8104-8115. DOI: 10.1021/acscatal.1c00874.
(14) Liu, S. B.; Kots, P. A.; Vance, B. C.; Danielson, A.; Vlachos, D. G. Plastic waste to fuels by hydrocracking at mild conditions. *Sci Adv* **2021**, *7* (17), 9, Article. DOI: 10.1126/sciadv.abf8283.

(15) Martín, A. J.; Mondelli, C.; Jaydev, S. D.; Pérez-Ramírez, J. Catalytic processing of plastic waste on the rise. *Chem-Us* **2021**, *7* (6), 1487-1533. DOI: 10.1016/j.chempr.2020.12.006.
(16) Wang, C.; Xie, T.; Kots, P. A.; Vance, B. C.; Yu, K.; Kumar, P.; Fu, J.; Liu, S.; Tsilomelekis, G.; Stach, E. A.; Zheng, W.; Vlachos, D. G. Polyethylene Hydrogenolysis at Mild Conditions over Ruthenium on Tungstated Zirconia. *Jacs Au* **2021**, *1* (9), 1422-1434. DOI: 10.1021/jacsau.1c00200.
(17) Zhang, F.; Zeng, M. H.; Yappert, R. D.; Sun, J. K.; Lee, Y. H.; LaPointe, A. M.; Peters, B.; Abu-Omar, M. M.; Scott, S. L. Polyethylene upcycling to long-chain alkylaromatics by tandem hydrogenolysis/aromatization. *Science* **2020**, *370* (6515), 437-441, Article. DOI: 10.1126/science.abc5441.
(18) Hongkailers, S.; Jing, Y.; Wang, Y.; Hinchiranan, N.; Yan, N. Recovery of Arenes from Polyethylene Terephthalate (PET) over a Co/TiO2 Catalyst. *Chemsuschem* **2021**, *14* (19), 4330-4339, DOI: https://doi.org/10.1002/cssc.202100956 (acccessed 2021/12/22).
(19) Jing, Y. X.; Wang, Y. Q.; Furukawa, S. Y.; Xia, J.; Sun, C. Y.; Hulsey, M. J.; Wang, H. F.; Guo, Y.; Liu, X. H.; Yan, N. Towards the Circular Economy: Converting Aromatic Plastic Waste Back to Arenes over a Ru/Nb2O5 Catalyst. *Angew Chem Int Edit* **2021**, *60* (10), 5527-5535. DOI: 10.1002/anie.202011063.
(20) Cheng, J. N.; Xie, J.; Xi, Y. J.; Wu, X. J.; Zhang, R. H.; Mao, Z. H.; Yang, H. F.; Li, Z. L.; Li, C. Selective Upcycling of Polyethylene Terephthalate towards High-valued Oxygenated Chemical Methyl p-Methyl Benzoate using a Cu/ZrO2 Catalyst. *Angew Chem Int Edit* **2024**, *63* (11). DOI: 10.1002/anie.202319896.

(21) Tang, H.; Hu, Y.; Li, G.; Wang, A.; Xu, G.; Yu, C.; Wang, X.; Zhang, T.; Li, N. Synthesis of jet fuel range high-density polycycloalkanes with polycarbonate waste. *Green Chem* **2019**, *21* (14), 3789-3795, 10.1039/C9GC01627A. DOI: 10.1039/C9GC01627A.
(22) Tang, H.; Li, N.; Li, G.; Wang, A.; Cong, Y.; Xu, G.; Wang, X.; Zhang, T. Synthesis of gasoline and jet fuel range cycloalkanes and aromatics from poly(ethylene terephthalate) waste. *Green Chem* **2019**, *21* (10), 2709-2719, 10.1039/C9GC00571D. DOI: 10.1039/C9GC00571D.
(23) Li, Y.; Wang, M.; Liu, X.; Hu, C.; Xiao, D.; Ma, D. Catalytic Transformation of PET and CO2 into High-Value Chemicals. *Angewandte Chemie International Edition* **2022**, *61* (e202117205). DOI: https://doi.org/10.1002/anie.202117205.
(24) Allendorf, M. D.; Stavila, V.; Snider, J. L.; Witman, M.; Bowden, M. E.; Brooks, K.; Tran, B. L.; Autrey, T. Challenges to developing materials for the transport and storage of hydrogen. *Nat Chem* **2022**, *14* (11), 1214-+. DOI: 10.1038/s41557-022-01056-2.
(25) Tran, B. L.; Johnson, S. I.; Brooks, K. P.; Autrey, S. T. Ethanol as a Liquid Organic Hydrogen Carrier for Seasonal Microgrid Application: Catalysis, Theory, and Engineering Feasibility. *Acs Sustain Chem Eng* **2021**, *9* (20), 7130-7138. DOI: 10.1021/acssuschemeng.1c01513.
(26) Müller, K.; Brooks, K.; Autrey, T. Releasing Hydrogen at High Pressures from Liquid Carriers: Aspects for the H2 Delivery to Fueling Stations. *Energ Fuel* **2018**, *32* (9), 10008-10015. DOI: 10.1021/acs.energyfuels.8b01724.
(27) Lu, S.; Jing, Y.; Feng, B.; Guo, Y.; Liu, X.; Wang, Y. H2-free Plastic Conversion: Converting PET back to BTX by Unlocking Hidden Hydrogen. *ChemSusChem* **2021**, *14* (19), 4242-4250. DOI: https://doi.org/10.1002/cssc.202100196.

(28) Gao, Z. W.; Ma, B.; Chen, S.; Tian, J. Q.; Zhao, C. Converting waste PET plastics into automobile fuels and antifreeze components. *Nat Commun* **2022**, *13* (1). DOI: ARTN 3343 10.1038/s41467-022-31078-w.

(29) Bai, X. S.; Aireddy, D. R.; Roy, A.; Ding, K. L. Solvent-Free Depolymerization of Plastic Waste Enabled by Plastic-Catalyst Interfacial Engineering. *Angew Chem Int Edit* **2023**, *62* (46). DOI: 10.1002/anie.202309949.
(30) Zeng, L.; Yan, T.; Du, J. J.; Liu, C. Y.; Dong, B.; Qian, B.; Xiao, Z.; Su, G. N.; Zhou, T.; Peng, Z. J.; Wang, Z. D.; Li, H. L.; Zeng, J. Recycling Valuable Alkylbenzenes from Polystyrene through Methanol-Assisted Depolymerization. *Angew Chem Int Edit* **2024**. DOI: 10.1002/anie.202404952.
(31) Larmier, K.; Liao, W. C.; Tada, S.; Lam, E.; Verel, R.; Bansode, A.; Urakawa, A.; Comas-Vives, A.; Copéret, C. CO2-to-Methanol Hydrogenation on Zirconia-Supported Copper Nanoparticles: Reaction Intermediates and the Role of the Metal-Support Interface. *Angew Chem Int Edit* **2017**, *56* (9), 2318-2323. DOI: 10.1002/anie.201610166.
(32) Hanukovich, S.; Dang, A.; Christopher, P. Influence of Metal Oxide Support Acid Sites on Cu-Catalyzed Nonoxidative Dehydrogenation of Ethanol to Acetaldehyde. *Acs Catal* **2019**, *9* (4), 3537-3550. DOI: 10.1021/acscatal.8b05075.
(33) Lam, E.; Corral-Prez, J. J.; Larmier, K.; Noh, G.; Wolf, P.; Comas-Vives, A.; Urakawa, A.; Copret, C. CO2 Hydrogenation on Cu/Al2O3: Role of Metal/Support Interface in Driving Activity and Selectivity of a Bifunctional Catalyst. *Angew Chem Int Edit* **2019**, *58* (39), 13989-13996. DOI: 10.1002/anie.201908060.
(34) Zhu, Y. F.; Zheng, J.; Ye, J. Y.; Cui, Y. R.; Koh, K.; Kovarik, L.; Camaioni, D. M.; Fulton, J. L.; Truhlar, D. G.; Neurock, M.; Cramer, C. J.; Gutiérrez, O. Y.; Lercher, J. A. Copper-zirconia interfaces in UiO-66 enable selective catalytic hydrogenation of CO2 to methanol. *Nat Commun* **2020**, *11* (1). DOI: ARTN 5849. 10.1038/s41467-020-19438-w.

(35) Cheng, G. H.; Jentys, A.; Gutiérrez, O. Y.; Liu, Y.; Chin, Y. H.; Lercher, J. A. Critical role of solvent-modulated hydrogen-binding strength in the catalytic hydrogenation of benzaldehyde on palladium. *Nat Catal* **2021**, *4* (11), 976-985. DOI: 10.1038/s41929-021-00701-2.
(36) Sha, F.; Tang, C. Z.; Tang, S.; Wang, Q. N.; Han, Z.; Wang, J. J.; Li, C. The promoting role of Ga in ZnZrO2 solid solution catalyst for CO2 hydrogenation to methanol. *J Catal* **2021**, *404*, 383-392. DOI: 10.1016/j.jcat.2021.09.030.

(37) Polliotto, V.; Livraghi, S.; Giamello, E. Electron magnetic resonance as a tool to monitor charge separation and reactivity in photocatalytic materials. *Research on Chemical Intermediates* **2018**, *44*, 3905-3921.
(38) Luo, X. J.; Liu, Y.; Yang, C.; Chen, S.; Tang, S.; Bärner, K. Oxygen vacancy related defect dipoles in CaCu3Ti4O12: detected by electron paramagnetic resonance spectroscopy. *Journal of the European Ceramic Society* **2015**, *35* (7), 2073-2081.
(39) Al'tshuler, S. A.; Kozyrev, B. M. *Electron paramagnetic resonance*; Academic Press, 2013.
(40) Ramaswamy, V.; Bhagwat, M.; Srinivas, D.; Ramaswamy, A. V. Structural and spectral features of nano-crystalline copper-stabilized zirconia. *Catalysis Today* **2004**, *97* (1), 63-70.
(41) Prasomsri, T.; Shetty, M.; Murugappan, K.; Román-Leshkov, Y. Insights into the catalytic activity and surface modification of MoO3 during the hydrodeoxygenation of

lignin-derived model compounds into aromatic hydrocarbons under low hydrogen pressures. *Energy Environ. Sci.* **2014**, *7* (8), 2660-2669, 10.1039/C4EE00890A. DOI: 10.1039/C4EE00890A.
(42) Shetty, M.; Anderson, E. M.; Green, W. H.; Román-Leshkov, Y. Kinetic analysis and reaction mechanism for anisole conversion over zirconia-supported molybdenum oxide. *J. Catal.* **2019**, *376*, 248-257. DOI: https://doi.org/10.1016/j.jcat.2019.06.046.
(43) Reid, R. C.; Prausnitz, J. M.; Poling, B. E. *The Properties of Gases and Liquids*; McGraw-Hill, 1987.
(44) Van Ness, H. C.; Abbott, M. M. *Classical Thermodynamics of Nonelectrolyte Solutions: With Applications to Phase Equilibria*; McGraw-Hill, 1982.
(45) Yang, M.; Yu, J. F.; Zimina, A.; Sarma, B. B.; Pandit, L.; Grunwaldt, J. D.; Zhang, L.; Xu, H. Y.; Sun, J. Probing the Nature of Zinc in Copper-Zinc-Zirconium Catalysts by Operando Spectroscopies for CO2 Hydrogenation to Methanol. *Angew Chem Int Edit* **2023**, *62* (7). DOI: 10.1002/anie.202216803.

(46) Jain, A.; Ong, S. P.; Hautier, G.; Chen, W.; Richards, W. D.; Dacek, S.; Cholia, S.; Gunter, D.; Skinner, D.; Ceder, G.; Persson, K. A. Commentary: The Materials Project: A materials genome approach to accelerating materials innovation. *APL Materials* **2013**, *1* (1), 011002. DOI: 10.1063/1.4812323 (acccessed 8/7/2024).
(47) Lempelto, A.; Gell, L.; Kiljunen, T.; Honkala, K. Exploring CO2 hydrogenation to methanol at a CuZn-ZrO2 interface via DFT calculations. *Catal Sci Technol* **2023**, *13* (15), 4387-4399. DOI: 10.1039/d3cy00549f.

(48) Kresse, G.; Furthmuller, J. Efficiency of ab-initio total energy calculations for metals and semiconductors using a plane-wave basis set. *Comp Mater Sci* **1996**, *6* (1), 15-50. DOI: Doi 10.1016/0927-0256(96)00008-0.
(49) Gražulis, S.; Merkys, A.; Vaitkus, A. Crystallography Open Database (COD). In *Handbook of Materials Modeling : Methods: Theory and Modeling*, Andreoni, W., Yip, S. Eds.; Springer International Publishing, 2018; pp 1-19.
(50) Grimme, S.; Ehrlich, S.; Goerigk, L. Effect of the Damping Function in Dispersion Corrected Density Functional Theory. *J Comput Chem* **2011**, *32* (7), 1456-1465. DOI: 10.1002/jcc.21759.
(51) de Saint Laumer, J.-Y.; Leocata, S.; Tissot, E.; Baroux, L.; Kampf, D. M.; Merle, P.; Boschung, A.; Seyfried, M.; Chaintreau, A. Prediction of response factors for gas chromatography with flame ionization detection: Algorithm improvement, extension to silylated compounds, and application to the quantification of metabolites. *Journal of Separation Science* **2015**, *38* (18), 3209-3217. DOI: https://doi.org/10.1002/jssc.201500106.
(52) Brunauer, S.; Emmett, P. H.; Teller, E. Adsorption of Gases in Multimolecular Layers. *Journal of the American Chemical Society* **1938**, *60* (2), 309-319. DOI: 10.1021/ja01269a023.
(53) Araujo, T. P.; Giannakakis, G.; Morales-Vidal, J.; Agrachev, M.; Ruiz-Bernal, Z.; Preikschas, P.; Zou, T. S.; Krumeich, F.; Willi, P. O.; Stark, W. J.; Grass, R. N.; Jeschke, G.; Mitchell, S.; López, N.; Pérez-Ramírez, J. Low-nuclearity CuZn ensembles on ZnZrO catalyze methanol synthesis from CO. *Nat Commun* **2024**, *15* (1). DOI: ARTN 3101. 10.1038/s41467-024-47447-6.

(54) Wang, Y. H.; Kattel, S.; Gao, W. G.; Li, K. Z.; Liu, P.; Chen, J. G. G.; Wang, H. Exploring the ternary interactions in Cu-ZnO-ZrO catalysts for efficient CO2 hydrogenation to methanol. *Nat Commun* **2019**, *10*. DOI: ARTN 1166 10.1038/s41467-019-09072-6.

(55) Kresse, G.; Hafner, J. Ab-Initio Molecular-Dynamics for Open-Shell Transition-Metals. *Phys Rev B* **1993**, *48* (17), 13115-13118. DOI: DOI 10.1103/PhysRevB.48.13115.
(56) Stadler, R.; Wolf, W.; Podloucky, R.; Kresse, G.; Furthmuller, J.; Hafner, J. Ab initio calculations of the cohesive, elastic, and dynamical properties of CoSi2 by pseudopotential and all-electron techniques. *Phys Rev B* **1996**, *54* (3), 1729-1734. DOI: DOI 10.1103/PhysRevB.54.1729.